RSC Advances

ROYAL SOCIETY OF CHEMISTRY

www.rsc.org/advances

Journal Name

COMMUNICATION

Ni/apatite-type lanthanum silicate supported catalyst in glycerol steam reforming reaction †

M. A. Goula,[a] N. D. Charisiou,[a] P. K. Pandis,[b] and V. N. Stathopoulos[b] *

Received 00th January 20xx,
Accepted 00th January 20xx

DOI: 10.1039/x0xx00000x

www.rsc.org/

In glycerol steam reforming reaction a 5wt% Ni/$La_{9.83}Si_{4.5}Fe_{1.5}O_{26\pm\delta}$ catalyst was found active and up to 3.2 times more selective to H_2 than a 5wt% Ni/Al_2O_3 catalyst, especially at low temperatures (<500°C). A H_2/CO molar ratio: 5 was achieved under a space velocity of 50000 h^{-1}.

Introduction

By 2020, the EU aims to have 10% of the transport fuel of every EU country coming from renewable sources such as biofuels. However, trans-esterification of fatty acids into biodiesel generates 10%w/w of glycerol as a by-product. As the biodiesel industry is blooming, the disposal of the crude glycerol produced in high amounts has become an emerging issue. Among various methods of crude glycerol disposal and utilization, glycerol steam reforming reaction (GSR) including chemical loop steam reforming appears as a potential alternative for renewable hydrogen production, with significant impact in the viability of numerous bio-refining processes and contribution to the rising need for renewable hydrogen. [1-5] The GSR has been investigated over various catalysts with supported Ru, Rh, Pt, Ni, Co and Fe proven to be active. Under similar conditions H_2 production yield reduced from Ru ~ Rh > Ni > Ir > Co > Pt > Pd > Fe. [5] Ni appears as the most promising active metal, due to its low cost, its ability towards O–H, C–H and C–C dissociation even more effectively than noble metals. [6,7] However Ni supported catalysts i.e. Ni/Al_2O_3, are found also to be susceptible to coke formation and active towards methanation reaction. [5] In steam reforming reactions catalytic performance is strongly affected by the nature of the supporting material. [5] The basicity, acidity, redox properties including oxygen mobility of the support and the dispersion of the active metal are crucial. [5,7] Mainly oxide and mixed oxide supports have been studied over GSR [5,6,8-10] and recently perovskites too. [11,12] Ni/Al_2O_3 is still considered as a viable state of the art catalyst for GSR.

Due to their physical-chemical and structural properties apatite-type lanthanum silicates (ATLS) have attracted research interest as promising intermediate temperature i.e. 600°C solid oxide fuel cell electrolytes. [13-22] They have interesting redox properties, oxygen mobility and a tuneable chemical composition, but their catalytic application studies appeared only recently either as supports for Pt in de-NO_X reaction [18,19] or as sole oxides in oxidative coupling of methane. [21] By changing the composition of ATLS i.e. Si with Al and/or Fe, an excess of interstitial oxygen ions in the lattice is generated or in the case of Fe, it can be stabilized in higher oxidation states just like in perovskite type oxides, with direct impact in catalytic properties. [22-25] In this work, we report for the first time ATLS as Ni support in GSR showing superior performance and selectivity than Ni/Al_2O_3 indicating a different reaction path possibly affected by ATLS very interesting oxygen solid state chemistry.

Results and Discussion

$La_{9.83}Si_{4.5}Fe_{1.5}O_{26\pm\delta}$ (LFSO) apatite was prepared in single phased hexagonal apatite structure (Fig.1S-"S" refers to Electronic Supplementary Information) and used as support material for a 5wt% Ni catalyst (Ni-LFSO), which was systematically studied for its catalytic performance for the GSR in a fixed bed reactor (Fig.4S). Comparative experiments with a 5wt% Ni supported on commercial γ-Al_2O_3 (Akzo) (Ni-ALO) and Ni-LFSO, as well as pure LFSO were performed under the same conditions. By XRD the LFSO and Ni-LFSO materials proved stable, showing apatite and NiO or Ni phases in their oxidative or reduced form, respectively. However, for the Ni-ALO nickel aluminate crystal

[a] Laboratory of Alternative Fuels and Environmental Catalysis, Department of Environmental and Pollution Control Engineering, School of Technological Applications, Technological Educational Institute of Western Macedonia, 50100, Koila, Kozani, Greece.
[b] Laboratory of Chemistry and Materials Technology, Department of Electrical Engineering, School of Technological Applications, Technological Educational Institute of Sterea Ellada, 34400 Psachna, Chalkida, Greece.
*Corresponding author: E-mail: vasta@teihal.gr; vasta@teiste.gr; Tel. +302228099688; +302228099621.
†Electronic Supplementary Information (ESI) available. See DOI: 10.1039/x0xx00000x

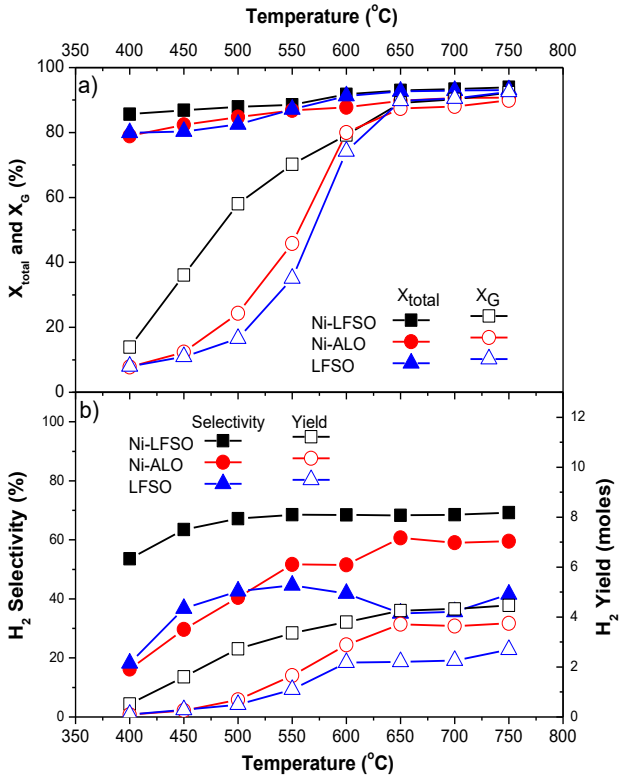

Figure 1. a) Total glycerol conversion (X_{total}; solid symbols) and glycerol conversion into gaseous products (X_G: open symbols) versus temperature. b) H_2 selectivity (solid symbols) and H_2 yield (open symbols) versus temperature for all samples tested. [Reaction conditions: $C_3H_8O_3$ (20 v/v %)/H_2O (total liquid flow rate = 0.12 ml/min)/ He=38 ml/min, $w_{catalyst}$=200 mg, T=400-750 °C].

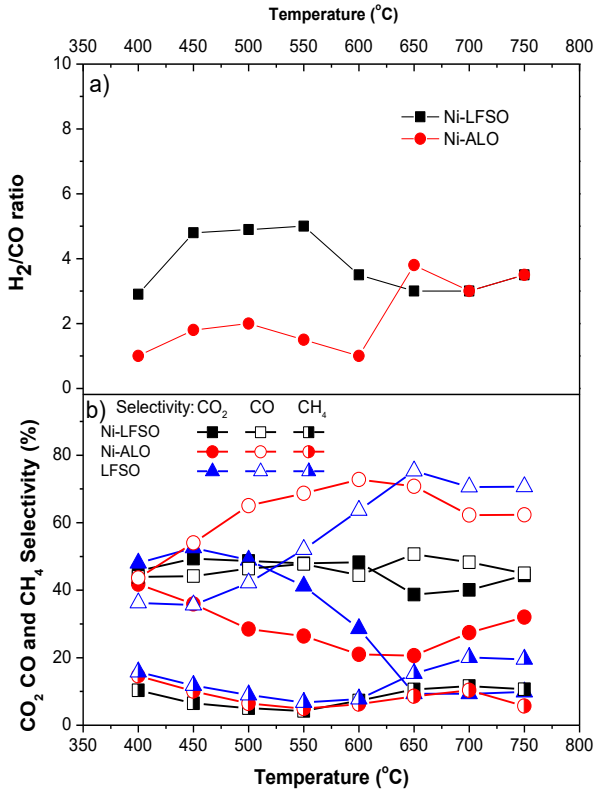

Figure 2. a) H_2/CO molar ratio, b) CO_2, CO and CH_4 selectivities versus temperature. [Reaction conditions: $C_3H_8O_3$ (20 v/v %)/H_2O (total liquid flow rate = 0.12 ml/min)/ He=38 ml/min, $w_{catalyst}$=200 mg, T=400-750 °C].

phase ($NiAl_2O_4$) was detected as expected. After reduction decreased intensities of Al_2O_3 and $NiAl_2O_4$ peaks and detection of the Ni^0 peaks was observed in Ni-ALO catalyst (Fig.1S). [26] However in Ni-ALO, $NiAl_2O_4$ species and Ni^0 coexist in contrast to Ni-LFSO. Main properties of materials (Table 1S), experimental conditions and all equations used for the calculations (Eq.1S-6S) can be found in Electronic Supplementary Information.

For Ni-ALO catalyst glycerol total conversion values increase from 79% at 400°C to 90% at 750°C. For LFSO conversion goes from 80% at 400°C to 93% at 750°C. When Ni is introduced to LFSO these values are improved to 86% - 94% respectively (Fig.1a). Glycerol conversion is high for the whole temperature range. On the other hand, its conversion to gaseous products increased with increasing temperature, ranging from 7.8%, 8% and 14% (400°C) to 90%, 93% and 94% (750°C) for Ni-ALO, LFSO and Ni-LFSO, respectively. Apatite shows significant activity towards gaseous products, but its performance is remarkably enhanced with Ni deposition, as Ni-LFSO.

Ni-LFSO catalyst shows a superior hydrogen selectivity (SH_2) that slightly increases with temperature (Fig.1b). Values range from 53.6% (400°C) to 69%% (750°C). Up to 500°C are found to be 3.2 to 1.7 times higher than Ni-ALO. In the whole reaction temperature range, the apatite supported catalytic sample revealed significantly higher hydrogen production comparing to the alumina one. Specifically, Ni-LFSO has reached a SH_2 value over 67% at reaction temperature as low as 500°C that remains almost stable until 750°C. Up to 500°C LFSO is found also more selective than Ni-ALO. At higher temperatures the LFSO selectivity to H_2 is suppressed. As for the yield towards H_2, it increases with temperature to the value of 4.5 for the Ni-LFSO, and 3.7 for the Ni-ALO, respectively. The superior performance of the apatite supported sample in comparison with the alumina one, at the low temperature range 450-550°C can be attributed to an enhanced contribution of the water gas shift (WGS) reaction that produces H_2 and CO_2 consuming CO and H_2O.

By performing the reaction with Water to Glycerol Feed Ratio (WGFR) equal to 9 the greatest quantity of hydrogen (6mol) is expected to be produced at 652°C. [10,27,28] In this study Ni-LFSO exhibits a H_2/CO molar ratio ranged from 3 to 5, with its highest value remaining almost stable for temperatures between 450-550°C. On the contrary, for the Ni-ALO sample the H_2/CO molar ratio takes values from 1 to 2 for the same temperature range. The high H_2 : CO ratio indicates that the WGS reaction ($CO + H_2O \rightarrow H_2 + CO_2$) is significantly favored in the case of the Ni-LFSO catalyst. By increasing the reaction temperature, H_2 fraction

improves more slowly than at lower temperature generating larger amounts of CO_2 and CO (Fig.2). [29]

We believe that the impressive performance of Ni-LFSO is related to its very interesting oxygen solid state chemistry. Interstitial and/or regular oxygen vacancies and the respective oxygen mobility is expected in ATLS materials. [13,16,17] As water is relatively difficult to be activated on the Ni sites [5,7] it may be activated in oxygen vacancies of the ATLS support, thus facilitating reforming reaction. On the counter back Ni-LFSO has limited surface area i.e. <2 m^2/g and consequently a very low metal dispersion is expected. Therefore a small interfacial area is expected between Ni and LFSO. Despite such features Ni-LFSO shows a glycerol conversion rate at 650°C of $2.55x10^{-2}$ $mmol \cdot g^{-1} \cdot s^{-1}$ or $1.27x10^{-2}$ $mmol \cdot m^{-2} \cdot s^{-1}$, while for Ni-ALO is $2.46x10^{-2}$ $mmol \cdot g^{-1} \cdot s^{-1}$ or $1.26x10^{-4}$ $mmol \cdot m^{-2} \cdot s^{-1}$ respectively. The above facts indicate Ni-LFSO active sites of impressive turnover reactivity. At lower reaction temperatures or if H_2 yield is considered, then values indicate further the superiority of Ni-LFSO catalytic surface. When LFSO was used without any Ni loading, reaction follows a different path which is clear above 500°C. No Ni sites are available to form adsorbed carbonyl groups and/or surface-bound proton, carbon, and oxygen species via dehydrogenation or cleavage of C–C bonds. Such intermediate species would eventually form CO_2 and H_2 through WGS reaction. On contrary for LFSO hydrogen selectivity is decreased in favor of CO and CH_4 production.

Similarly, a very different behavior can be observed between our catalysts towards the liquid products selectivities. For the Ni-ALO catalyst (Fig 3b) the main liquid products were: (i) acetol for T< 600°C with a maximum value of 45% at 500°C, (ii) acetone with selectivity values ranging from 20 (400°C) to 70% (650°C) and (iii) allyl alcohol, acetaldehyde and acetic acid with quite constant values at 10-15% for temperatures lower than 650°C. The most interesting observation is that no condensates were detected for reaction temperatures higher than 650°C.

A quite different liquid products' profile is observed for the Ni-LFSO catalyst (Fig 3a) as follows: (i) acetol with a rather constant selectivity value of 30% up to 600°C and a decreasing trend in higher temperatures, (ii) acetone with selectivity values ranging from 14% (400°C) to 24% (750°C), (iii) allyl alcohol with selectivity values ranging between 24-34% for the whole temperature range and (iv) acetaldehyde and acetic acid with selectivity values ranging from 15 and 9% (400°C) to 22 and 20% (750°C), respectively. It should be also emphasized that in contrast to the Ni-ALO sample, all of the main liquid products were detected at reaction temperature as high as 750°C. LFSO catalyst shows similar to Ni-LFSO liquid products mainly up to 600°C. Above 600°C acetol production is drastically decreased in favor of acetone. Allyl alcohol production is rather stable (Fig.3c). These findings are in accordance with the literature, as Araque et al. [29] have also found that condensable products such as acetol, acetaldehyde, and propenal (allyl alcohol precursor) were produced during the steam reforming of glycerol, but they were considered as precursors of coke formation. [1, 30] At the low temperature range (<600°C) for which the production of liquids seems to be significant for the Ni-ALO catalyst the reaction proceeds through the path of acetol intermediate to acetone (Fig.5S). On the contrary, for the Ni-LFSO and LFSO catalyst the

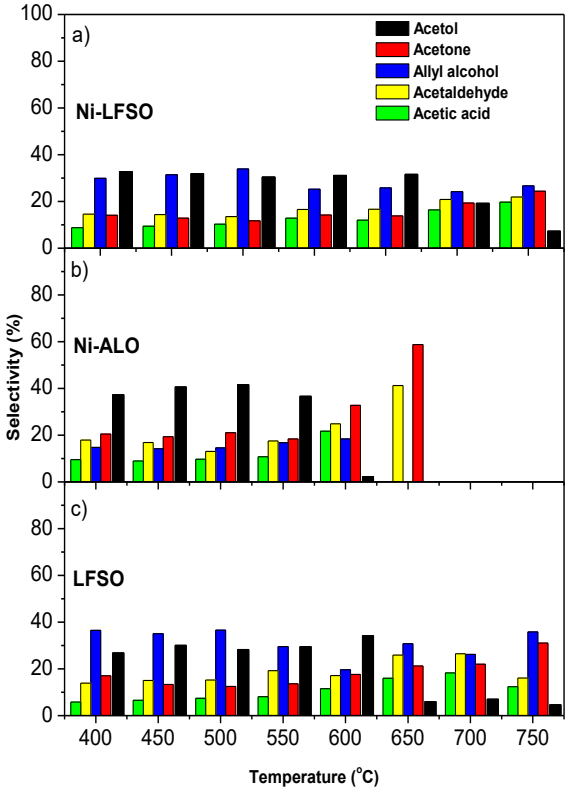

Figure 3. Liquid products' selectivities versus temperature: (a) Ni-LFSO, (b) Ni-ALO and (c) LFSO samples. [Reaction conditions: $C_3H_8O_3$ (20 v/v %)/H_2O (total liquid flow rate = 0.12 ml/min)/ He=38 ml/min, $w_{catalyst}$=200 mg, T=400-750 °C].

reaction rather proceeds in parallel pathways via acetol intermediate producing acetone and via propenal producing allyl alcohol. These results clearly indicate a different mechanism of glycerol activation in such reforming reaction conditions. This variation is in agreement with the different behavior observed towards H_2 production. Also a different carbon accumulation route to the catalytic surface is expected.

According to the TGA technique, applied on spent catalysts, approximately 25wt% of carbon accumulation (Fig.2S) was found for both Ni catalytic samples. However, a very different thermal decomposition profile is found. This is an indication of the varying condensate species formed as reaction intermediates for the Ni-ALO and Ni-LFSO catalysts. This carbon is extensively accumulated on the surface of the catalytic samples (see SEM images in Fig.3S). According to the literature [31-33], the cleavage of the C–C or C–O bonds in the molecule of glycerol can be achieved only through a dehydrogenation step taking place on the metal active sites and the production of intermediates on the catalytic surface. Moreover, the formation of CO and H_2 is mainly due to the strong capacity of Ni catalysts in the breaking of the C–C bond. From the thermodynamic point of view, the steam reforming reaction is limited at low temperatures, while the water-gas shift (WGS) and methanation reactions are favored. Thus, a higher contribution of

the steam reforming reaction, compared with the glycerol decomposition when the temperature increases, is suggested by our results, too.

About Ni-Al_2O_3 catalysts, Valliyappan et al. [34] suggested that glycerol steam reforming goes though the dissociative adsorption of the glycerol and water molecules to Ni and Al_2O_3 sites, respectively. Consequently, H_2 produced via dehydrogenation of the chemisorbed glycerol, as well as through reactions between the adsorbed organic fragments and Al_2O_3 surface hydroxyl groups. On the other side, a reaction scheme composed of two parallel pathways; one containing glycerol dehydration and dehydrogenation at the outset, while the other initiates with solely dehydrogenation was proposed by the Nichio's group. [35,36] They also suggested total conversion of the intermediates, such as acetol and acetaldehyde through the dehydrogenation, hydrogenolysis and WGS reactions, while coke formation depends on high molecular weight compounds (e.g., phenol) condensation. Adapting the idea of reactant's dissociative adsorption on the Ni-based catalysts surface and correlating the mechanistic studies with Langmuir-Hinshelwood kinetics led Cheng et al. to the conclusion that this must be considered as the whole process' rate-limiting step. [37] In the case of Ni-ATLS a redox mechanism over the available oxygen vacancies may be assumed. [33] Water may adsorb and be activated as surface hydroxyls over such vacancies reducing ATLS surface. Thus, reduced ATLS may interact with the dehydrogenation intermediate species from Ni to form CO_2 and H_2, closing the redox cycle of ATLS in WGS. However another coexisting mechanism cannot be excluded explaining the dual path of glycerol reaction via acetol and propenal. An operando approach can shed light on the underlying mechanism but is outside the scope of the present communication.

Conclusions

ATLS show impressive performance as a support boosting the performance of Ni-based catalysts in the GSR. Despite the much lower specific surface area of ATLS compared to Al_2O_3 support and their eventually larger Ni crystallites they exhibit excellent low temperature conversion rates and selectivity towards H_2 production. Ni-ATLS superior performance can be attributed to the existence of a redox GSR mechanism. Such a redox catalyst enables mobility and storage of lattice oxygen, by which water dissociation and WGS can be enhanced, to high H_2 yield. Further work is ongoing in order to shed light upon the role of the interesting ATLS group of materials as Ni supports as well as their compositional effect in GSR.

Acknowledgements

Financial support by the programs THALIS and Archimedes III implemented within the framework of Education and Lifelong Learning Operational Programme, co-financed by the Hellenic Ministry of Education, Lifelong Learning and Religious Affairs and the European Social Fund, Projects: 'Production of Energy Carriers from Biomass by Products. Glycerol Reforming for the Production of Hydrogen, Hydrocarbons and Superior Alcohols' and 'Synthesis, characterization and study of properties of solid electrolytes of the apatite structure for fuel cell applications', is gratefully acknowledged. Moreover, the authors also wish to acknowledge financial support provided by the Committee of the Special Account for Research Funds of the Technological Educational Institute of Western Macedonia (ELKE, TEIWM, Grant number: 80126).

References

1 A. Corma, G. Huber, L. Sauvanaud and P. Oconnor, *J. Catal.*, 2008, 257, 163-171.
2 G. Nahar and V. Dupont, Biofuels, 2012, 3, 167–191.
3 N.D. Charisiou, O.A. Bereketidou, M.A. Goula, *4th International Symposium on Energy from Biomass and Waste*, Venice, Italy, 2012, November 12-15.
4 J.M. Silva, M.A. Soria, L.M. Madeira, *Renew. Sust. Energ. Rev.*, 2015, 42, 1187-1213.
5 N. H. Tran and G. S. Kannangara, *Chem. Soc. Rev.* , 2013, 42, 9454-9479
6 K.N. Papageridis, G.Siakavelas, N.D. Charisiou, D.G. Avraam, L.Tzounis, K. Kousi, M.A. Goula, *Fuel Proc. Tech.* 2016, 152, 156–175.
7 S. Li and J. Gong, *Chem. Soc. Rev.*, 2014, 43, 7245-7256
8 L.V. Matoos, G. Jacobs, B.H. Davis, F.B. Noronha, *Chime. Rev.*, 2012, 112, 4094.
9 S. Adhikari, S.D. Fernando, S.D.F. To, R.M. Bricka, S P.H. Steele, A.Haryanto, *Energy Fuels*, 2008, 22, 1220–1226.
10 A. Iriondo, V. L. Barrio, J. F. Cambra, P. L. Arias, M. B. Güemez, R. M. Navarro, M. C. Sánchez-Sánchez and J. L. G. Fierro, *Top. Catal.*, 2008, 49, 46-58.
11 G. Wu, S. Li, C. Zhang, T. Wang and J. Gong, *Appl. Catal., B*, 2014, 144, 277-28.
12 M. Surendar, T. V. Sagar, B. H. Babu, N. Lingaiah, K. S. Rama Rao and P. S. S. Prasad, *RSC Adv.*, 2015, 5, 45184-45193.
13 T. Kharlamova, O. Vodyankina, A. Matveev, V. Stathopoulos, A. Ishchenko, D. Khabibulin and V. Sadykov , *Ceram. Int.*, 2015, 41, 13393-13408.
14 K. Kobayashi, Y.Sakka, *J. Ceram. Soc. Jpn.*, 2014, 122, 921–939.
15 H. Gasparyan, C. Argirusis, C. Szepanski, G. Sourkouni, V. Stathopoulos, T. Kharlamova, V. A. Sadykov and S. Bebelis , *ECS Trans.*, 2009, 25, 2681-2688.
16 H. Gasparyan, S. Neophytides, D. Niakolas, V. Stathopoulos, T. Kharlamova, V. Sadykov, O. Van der Biest, E. Jothinathan, E. Louradour, J. P. Joulin and S. Bebelis , *Solid State Ionics*, 2011, 192, 158-162.
17 V. Sadykov, E. Sadovskaya, A. Bobin, T. Kharlamova, N. Uvarov, A. Ulikhin, C. Argirusis, G. Sourkouni and V. Stathopoulos , *Solid State Ionics*, 2015, 271, 69-72.
18 S. Kato, T. Yoshizava, N. Kakuta, S. Akiyama, M. Okasawara, T. Wakabayashi, Y. Nakahara and S. Nakata , S., *Res. Chem. Intermed*, 2008, 34, 703-708.
19 T. Wakabayashi, S. Kato, Y. Nakahara, M. Ogasawara and S. Nakata, *Catal. Today*, 2011, 164, 575-579.
20 X. H. Zhang, X. Yi, J. Zhang, Z. Xie, J. Kang and L. Zheng , *Inorg. Chem.*, 2010, 49, 10244-10246.

21 T. S. Kharlamova, A. S. Matveev, A. V. Ishchenko, A. N. Salanov, S. V. Koshcheev, A. I. Boronin and V. A. Sadykov, *Kinet. Catal.*, 2014, 55, 361-371.
22 P.K.Pandis, E.Xenogiannopoulou, P.M.Sakkas, G.Sourkouni, C.Argirusis, V.N.Stathopoulos, *RSC Adv.*, 2016, 6, 49429–49435.
23 V. V. Kharton, A. L. Shaula, M. V. Patrakeev, J. C. Waerenborgh, D. P. Rojas, N. P. Vyshatko, E. V. Tsipis, A. A. Yaremchenko and F. M. B. Marques, *J. Electrochem. Soc.*, 2004, 151, A1236.
24 V. Sadykov, T. Kharlamova, S. Pavlova, V. Muzykantov, A. Ishchenko, T. Krieger, O. Lapina, N. Uvarov, M. Chaikina, Yu. Pavlyukhin, Ch. Argirusis, S. Bebelis, H. Gasparyan, V. Stathopoulos, E. Jothinathan, O. Van der Biest, *Lanthanum Compounds, Production and Applications*, *Nova Science Publishers, Inc., Hauppauge, NY,* 2010, pp. 1-126.
25 V. N. Stathopoulos, V. C. Belessi, T. V. Bakas, S. G. Neophytides, C. N. Costa, P. J. Pomonis and A. M. Efstathiou, *Appl. Catal., B* , 2009, 93, 1-11.
26 L. F. Bobadilla, A. Penkova, A. Álvarez, M. I. Domínguez, F. Romero-Sarria, M. A. Centeno and J. A. Odriozola , *Appl. Catal.*, A, 2015, 492, 38-47.
27 X.D. Wang, S.R. Li, H. Wang, B. Liu, X.B. Ma, *Energ. Fuels*, 2008, 22, 84285-84291.
28 S. Adhikari, S. Fernando, S.R. Gwaltney, S.D. Filip To, R.M. Bricka, P.H. Steele, A. Haryanto, *Int. J. Hydr. Energy,* 2007, 32, 2875 – 2880
29 M. Araque, L. M. Martínez T, J. C. Vargas, M. A. Centeno and A. C. Roger , *Appl. Catal., B*, 2012, 125, 556-566.
30 J. Barrault, J.-M. Clacens and Y. Pouilloux, *Top. Catal.*, 2004, 27, 137-142.
31 R.D. Cortright, R.R. Davda, J.A.Dumesic, *Nature*, 2002, 418, 964-967.
32 S. Adhikari, S. D. Fernando and A. Haryanto, A., *Renew. Energ*., 2008, 33, 1097-1100.
33 B. Zhang, X. Tang, Y. Li, Y. Xu and W. Shen , *Int. J. Hydrogen Energy*, 2007, 32, 2367-2373.
34 T. Valliyappan, D. Ferdous, N. N. Bakhshi and A. K. Dalai, *Top. Catal.*, 2008, 49, 59-67.
35 F. Pompeo, G. F. Santori and N. N. Nichio, *Catal. Today*, 2011, 172, 183-188.
36 F. Pompeo, G. F. Santori and N. N. Nichio , *Int. J. Hydrogen Energy*, 2010, 35, 8912-8920.
37 C. K. Cheng, S. Y. Foo and A. A. Adesina, *Ind. Eng. Chem. Res.*, 2010, 49, 10804–10817.

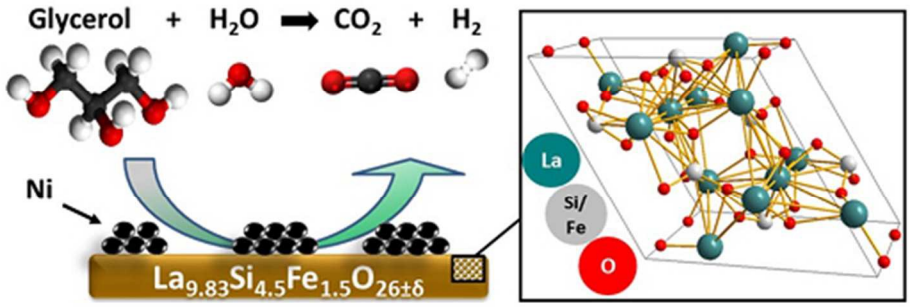

74x39mm (192 x 192 DPI)